Research Square

Preprints are preliminary reports that have not undergone peer review.
They should not be considered conclusive, used to inform clinical practice,
or referenced by the media as validated information.

Urban Heat Island Dynamics and 2030 Thermal Scenario in Pokhara, Nepal Using Landsat and CA–Markov Modeling

Bhuwan Singh Bisht

geo.bhuwan@gmail.com

Land Management Training Center

Dr. Hemu Kafle

Kathmandu institute of Applied Sciences

Amit Yadav

Kathmandu University

Sushil Subedi

Kathmandu University

Gaurav Bisht

Kathmandu University

Research Article

Keywords: Urban Heat Island, Land Surface Temperature, Land Use/Land Cover, Landsat, CA–Markov, Pokhara, Remote Sensing

Posted Date: August 24th, 2026

DOI: https://doi.org/10.21203/rs.3.rs-10534483/v1

License: This work is licensed under a Creative Commons Attribution 4.0 International License.
Read Full License

Additional Declarations: No competing interests reported.

Urban Heat Island Dynamics and 2030 Thermal Scenario in Pokhara, Nepal Using Landsat and CA–Markov Modeling

Bhuwan Singh Bisht[1,2]*, Dr. Hemu Kafle[3], Amit Yadav[4], Sushil Subedi[4], Gaurav Bisht[4]

[1] Land Management Training Center, Dhulikhel, Nepal
[2] Nepal Open University, Lalitpur, Nepal
[3] Kathmandu institute of Applied Sciences, Lalitpur, Nepal
[4] Kathmandu University, Dhulikhel, Nepal
Bhuwan Singh Bisht (https://orcid.org/0009-0009-2669-2475)
Dr. Hemu Kafle (https://orcid.org/0000-0003-3981-0417)
Amit Yadav (https://orcid.org/0009-0002-1155-1142)
Sushil Subedi (https://orcid.org/0009-0007-3980-5948)
Gaurav Bisht (https://orcid.org/0009-0002-8040-9350)

Corresponding Author Bhuwan Singh Bisht (geo.bhuwan@gmail.com)

Abstract

Urban heat islands are an increasing concern in rapidly urbanizing cities where vegetation and cultivated land are being converted into impervious and exposed surfaces. This study assessed land use/land cover change, vegetation condition, land surface temperature, and urban heat island intensity in the 37.42 km² core urban area of Pokhara Metropolitan City, Nepal. Landsat imagery from 2014, 2019, and 2024 was processed in Google Earth Engine. Support Vector Machine classification was used for land-cover mapping, while NDVI and EVI were used to examine vegetation conditions. Landsat-derived land surface temperature was evaluated using MODIS LST, and DHM air-temperature records were used as supplementary thermal-consistency evidence. A CA–Markov model was applied to generate a 2030 land-cover scenario and assess its likely thermal implications. Results showed that settlement increased from 20.01% in 2014 to 37.45% in 2024, while cultivation declined from 78.04% to 55.53%. Mean land surface temperature increased from 29.87°C to 37.46°C, and maximum temperature increased from 36.19°C to 44.58°C. Landsat LST showed reasonable agreement with MODIS LST, with a correlation coefficient of 0.736 and RMSE of 2.79°C. The 2030 scenario suggests that settlement and airport-related built-up surfaces may occupy 50.43% of the study area, while High and Extremely High UHI classes

may together cover 50.63%. The findings highlight the need for urban greening, exposed-surface management, and heat-sensitive planning in Pokhara.

Keywords: *Urban Heat Island; Land Surface Temperature; Land Use/Land Cover; Landsat; CA–Markov; Pokhara; Remote Sensing*

Introduction

Rapid urbanization is one of the major processes transforming the physical and environmental characteristics of cities. The conversion of vegetation, cultivated land, water-influenced surfaces, and open spaces into buildings, roads, transportation corridors, airport infrastructure, barren land, and other impervious or exposed surfaces alters surface reflectance, heat storage, moisture availability, and energy exchange between the land surface and the atmosphere. These changes can intensify urban thermal conditions and contribute to the development of Urban Heat Island (UHI) effects, where urbanized surfaces become warmer than surrounding vegetated or less-developed areas [1,2].

Land Surface Temperature (LST) derived from thermal remote sensing has become an important indicator for analysing urban thermal environments. Unlike station-based air temperature, which represents near-surface atmospheric temperature at specific locations, satellite-derived LST represents the radiometric temperature of surface materials such as roads, rooftops, bare soil, cultivated fields, vegetation, water bodies, and airport surfaces [2,3]. Therefore, LST provides spatially continuous information for identifying urban thermal hotspots and examining how land-cover transformation influences surface heating.

Vegetation plays a key role in regulating urban surface temperature. Vegetated surfaces reduce heating through shading, evapotranspiration, and moisture retention, whereas impervious and exposed surfaces generally absorb and store more solar energy. The Normalized Difference Vegetation Index (NDVI) and Enhanced Vegetation Index (EVI) are widely used to assess vegetation greenness and condition in relation to surface temperature [4,5]. Previous studies have shown that areas with higher vegetation-index values generally have lower LST, while built-up, barren, exposed, and sparsely vegetated surfaces tend to show higher surface temperatures [3,6].

Several studies have linked land use/land cover (LULC) change with increasing urban thermal stress. In Nepal, studies conducted in Kathmandu Valley have reported higher LST in impervious, barren, open, and airport-related areas, while vegetation-dominated surfaces showed comparatively lower temperatures [6,7]. These findings indicate that urban heat is influenced not only by dense settlement but also by exposed land, construction areas, road corridors, and large impervious surfaces. Recent research in Pokhara has also reported warmer conditions in urban areas compared with less-developed and vegetation-dominated locations, showing the emerging importance of UHI analysis in the city [8].

Pokhara Metropolitan City is undergoing rapid urban and infrastructural development. However, the complete administrative boundary of Pokhara includes extensive rural settlements, agricultural land, forests, hills, lakes, river valleys, and less-developed peripheral areas. Analysing the entire municipal area may dilute the thermal signal associated with concentrated urban growth. Therefore, a focused assessment of the core urban area is necessary to understand how settlement expansion, cultivation decline, vegetation fragmentation, airport-related infrastructure, barren land, and exposed surfaces influence LST and UHI intensity within the most rapidly urbanizing part of the city.

Although previous studies have examined urban heat and land-cover change in Nepal, limited research has integrated multi-temporal LULC classification, vegetation-index analysis, class-wise LST assessment, standardized UHI mapping, satellite-based LST evaluation, station-based thermal-consistency assessment, and near-future thermal scenario analysis within the core urban area of Pokhara. Such an integrated approach is important for identifying historical thermal changes as well as possible future heat-risk zones under continued urban expansion. Scenario-based modelling can provide useful spatial evidence for climate-sensitive urban planning, even though future thermal outputs should not be interpreted as exact forecasts.

This study therefore analyses LULC change, NDVI, EVI, LST, and standardized UHI intensity in the selected 37.42 km² core urban area of Pokhara Metropolitan City using Landsat imagery for 2014, 2019,

and 2024. Landsat-derived LST is evaluated using MODIS LST, while air-temperature records from Pokhara Airport Station are used only as supplementary thermal-consistency evidence because LST and air temperature represent different physical measurements. The study further applies the CA–Markov model to generate a 2030 LULC scenario and assess its likely thermal implications. Specifically, the study aims to assess spatiotemporal changes in LULC, vegetation condition, LST, and UHI intensity; examine the relationship between vegetation, land-cover classes, and surface thermal patterns; evaluate the reliability of Landsat-derived LST using MODIS and supplementary DHM records; and explore the possible 2030 land-cover and UHI scenario to support climate-sensitive planning and urban heat mitigation in Pokhara.

2. Materials and Methods

2.1 Study area

This study was conducted in the selected 37.42 km² core urban area of Pokhara Metropolitan City, Kaski District, Gandaki Province, Nepal. The selected area includes all or parts of Wards 1–18 and Ward 22 and represents the continuously developed and rapidly urbanizing part of the city. The analysis focused on the core urban area rather than the complete municipal boundary because the wider municipality includes extensive agricultural land, forests, hills, lakes, river valleys, rural settlements, and less-developed peripheral areas, which could dilute the thermal signal of concentrated urban development.

The study area contains dense settlements, commercial areas, major road corridors, airport infrastructure, cultivated land, forest patches, water bodies, barren land, construction areas, and exposed surfaces. These land-cover types have different thermal characteristics, making the area suitable for analysing the relationship between land-cover transformation, vegetation condition, land surface temperature, and urban heat island intensity. All area-based analyses were carried out using the WGS 1984 UTM Zone 45N projected coordinate system.

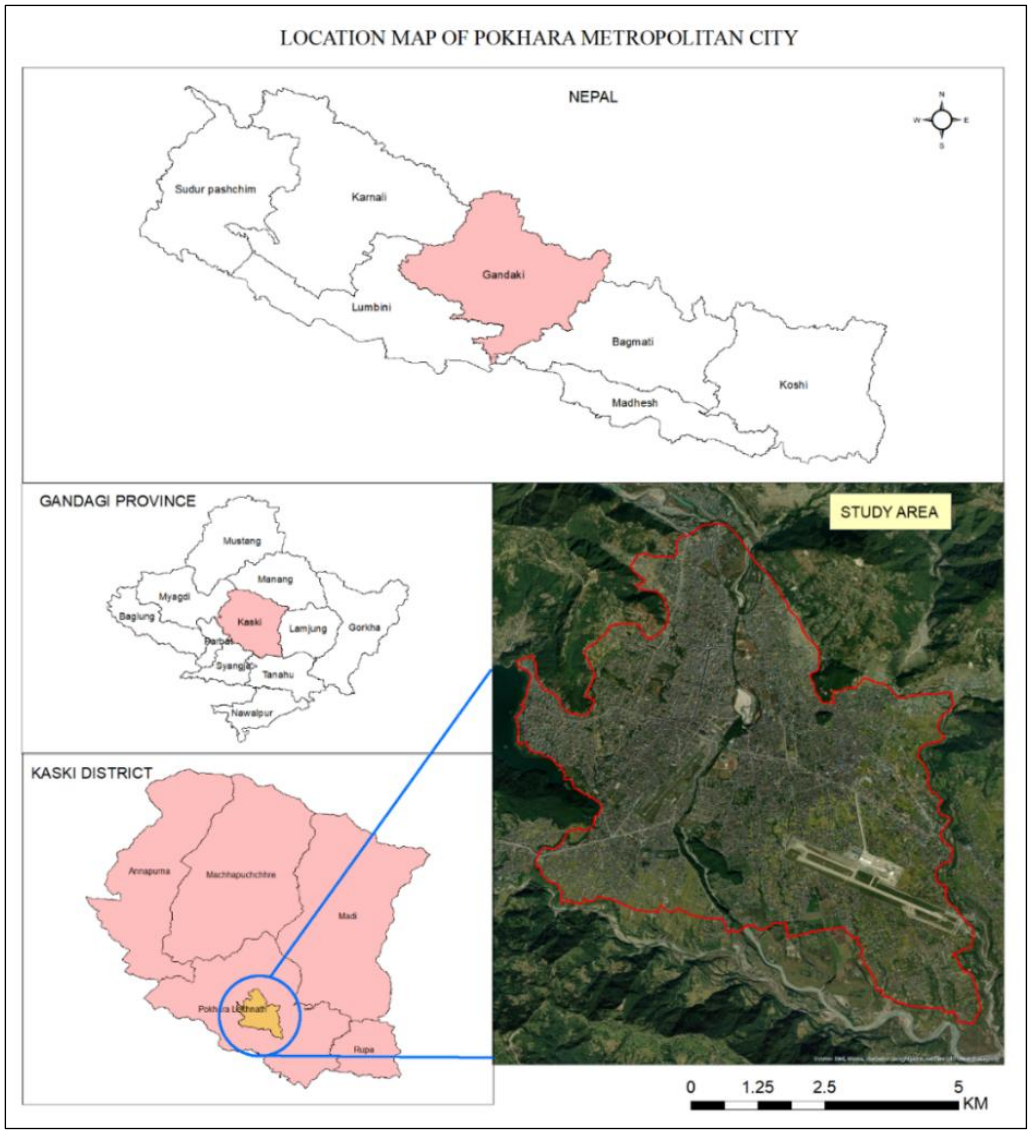


Fig. 1 Study area showing the selected core urban area of Pokhara Metropolitan City

2.2 Data sources and preprocessing

This study used satellite imagery, administrative boundary data, MODIS LST data, classified land-cover maps, and station-based air-temperature records. The details of the datasets, sources, periods, spatial or temporal resolution, and their purposes are summarized in Table 1. Landsat imagery was used for LULC classification, vegetation-index calculation, LST retrieval, and UHI mapping. MODIS LST was used for cross-sensor evaluation of Landsat-derived LST, while air-temperature records from the Department of Hydrology and Meteorology were used only for supplementary thermal-consistency assessment.

Landsat Collection 2 Level 2 imagery was accessed and processed in Google Earth Engine [9]. Landsat 8 OLI/TIRS imagery was used for 2014 and 2019, while Landsat 8/9 OLI/TIRS imagery was used for 2024 depending on image availability and cloud condition. Images acquired between March and May were selected to maintain seasonal consistency among the study years. This pre-monsoon period was used to reduce the effects of monsoon rainfall, winter cooling, and major seasonal vegetation differences.

Clouds, cloud shadows, cirrus, snow, saturated pixels, and invalid observations were removed using the QA_PIXEL and QA_RADSAT bands. Optical surface-reflectance bands and the thermal surface-temperature band were scaled according to Landsat Collection 2 Level 2 specifications. The same study boundary and seasonal window were maintained for all study years to improve spatial and seasonal comparability.

Table 1 Data sources used in the study

SN	Data	Source/Platform	Period	Spatial / Temporal Resolution	Purpose
1	Administrative Boundary	National Geoportal of Nepal	Current boundary	Vector boundary data	Delineation of the study area boundary
2	Landsat 8/9 OLI/TIRS	Google Earth Engine	2024	30 m optical bands; thermal data processed/resampled to 30 m	LULC classification, spectral index calculation, LST estimation, and UHI analysis
3	Landsat 8 OLI/TIRS	Google Earth Engine	2014 and 2019	30 m optical bands; thermal data processed/resampled to 30 m	LULC classification, spectral index calculation, LST estimation, and UHI analysis
4	MODIS LST Data	Google Earth Engine	Corresponding validation period	Approximately 1 km	Evaluation of Landsat-derived LST
5	LULC Maps	Supervised classification in Google Earth Engine	2014, 2019, and 2024	30 m	Preparation of land use/land cover maps for 2014, 2019, and 2024

6	Monthly Air-Temperature Records	Department of Hydrology and Meteorology	2014, 2019, and 2024	Station-based point data; monthly temporal resolution	Station-based thermal-consistency assessment

2.3 Land use/land cover classification

Supervised LULC classification was carried out for 2014, 2019, and 2024 using the Support Vector Machine algorithm. SVM was selected because it can separate spectrally complex land-cover classes in heterogeneous urban environments [10]. Training samples were prepared through visual interpretation of Landsat composites and available high-resolution reference imagery. Samples were distributed across the study area to represent the spectral variability within each class.

Five LULC classes were used: settlement, cultivation, forest, water bodies, and barren land. Settlement included buildings, roads, commercial areas, institutional areas, airport infrastructure, and other major impervious surfaces. Cultivation represented agricultural fields and actively or recently cultivated land. Forest represented tree-dominated and comparatively dense vegetation. Water bodies included lakes, rivers, ponds, and permanent surface-water features. Barren land represented exposed soil, construction areas, dry open surfaces, and sparsely vegetated land.

After classification, the outputs were visually inspected, and post-classification filtering was applied to reduce isolated pixels and improve spatial consistency. Accuracy assessment was conducted using a confusion matrix. Overall Accuracy and Kappa coefficient were calculated to evaluate the reliability of the classified maps.

2.4 Vegetation indices

NDVI and EVI were calculated from scaled Landsat surface-reflectance bands to assess vegetation distribution, greenness, and condition. NDVI was used to represent vegetation greenness, while EVI provided additional sensitivity to vegetation condition and helped reduce some soil-background and atmospheric effects [4,5]. NDVI was calculated following Tucker [5] as:

$$\mathrm{NDVI} = \frac{\mathrm{NIR} - \mathrm{Red}}{\mathrm{NIR} + \mathrm{Red}}$$

where NIR is the near-infrared surface reflectance and Red is the red-band surface reflectance. Higher NDVI values generally indicate denser and healthier vegetation, while lower values indicate settlement, exposed land, barren land, water, or sparse vegetation. EVI was calculated following Huete et al. [4] as:

$$\mathrm{EVI} = \mathrm{G} * \frac{(\mathrm{NIR} - \mathrm{Red})}{(\mathrm{NIR} + C_1 * \mathrm{Red} - C_2 * \mathrm{Blue} + \mathrm{L})}$$

where NIR, Red, and Blue represent the corresponding Landsat surface-reflectance bands. The coefficients used were G=2.5, C_1=6, C_2=7.5, and L=1. Higher EVI values indicate stronger vegetation condition, whereas lower values indicate sparse vegetation, settlement, exposed land, or water.

2.5 Land surface temperature retrieval

Land Surface Temperature (LST) was derived from the Landsat Collection 2 Level 2 Surface Temperature band. For Landsat 8/9, the ST_B10 band was used. The scaled pixel values were converted into Kelvin using the scale factor and offset recommended by the United States Geological Survey for Landsat Collection 2 Level 2 surface temperature products [11]. The Kelvin values were then converted into degrees Celsius

LST (K)= ST_B10 * 0.00341802 + 149.0

LST(°C) = LST(K)−273.15

The resulting LST raster was clipped to the selected study area and used for multi-temporal comparison, class-wise LST analysis, MODIS-based evaluation, station-based thermal-consistency assessment, and standardized UHI mapping.

2.6 Urban heat island mapping

Urban Heat Island intensity was calculated using the standardized deviation of pixel-level LST from the mean LST of each annual image. This approach was used to identify relative thermal-intensity zones within the study area and was calculated following Abutaleb et al. [12] as:

$$\mathrm{UHI} = \frac{\mathrm{T_s} - \mathrm{T_m}}{\mathrm{SD}}$$

where T_s is the LST of an individual pixel, T_m is the mean LST of the image, and SD is the standard deviation of LST. The resulting UHI values are dimensionless and represent relative thermal intensity. They do not represent direct urban–rural temperature differences in degrees Celsius.

The standardized UHI maps were classified into five thermal-intensity classes: Extremely Low, Low, Moderate, High, and Extremely High. These classes were used to examine the spatial distribution and temporal expansion of relative thermal hotspots in 2014, 2019, and 2024.

2.7 Evaluation of Landsat-derived LST

Landsat-derived LST was evaluated using the MOD11A1.061 Terra Land Surface Temperature product [14]. MODIS provides daily LST observations at approximately 1 km spatial resolution, whereas Landsat-derived LST provides more detailed spatial information at 30 m resolution. To enable comparison, Landsat-derived LST was resampled to 1000 m resolution, and corresponding valid pixels were extracted from both Landsat and MODIS datasets.

The agreement between Landsat and MODIS LST was assessed using Pearson's correlation coefficient and Root Mean Square Error. Pearson's correlation coefficient was used to examine whether both datasets captured a similar spatial thermal pattern, while RMSE was used to measure the average magnitude of difference between paired observations [15].

DHM air-temperature records from Pokhara Airport Station were used as supplementary thermal-consistency evidence. These records were not used as direct validation of Landsat-derived LST because air temperature and land surface temperature represent different physical measurements [16]. Landsat LST represents the radiometric temperature of surface materials, whereas DHM air temperature represents near-surface atmospheric temperature measured at approximately two metres above ground level.

For the available years, Landsat LST extracted at the station location was compared with March–May DHM maximum air temperature and mean air temperature. Mean Error, Mean Absolute Error, and RMSE were calculated to describe the numerical difference between satellite-derived surface temperature and station-recorded air temperature.

$$ME = \frac{1}{n}\sum_{i=1}^{n} \quad (LST_i - T_{air,i})$$

$$MAE = \frac{1}{n}\sum_{i=1}^{n} |LST_i - T_{air,i}|$$

$$RMSE = \sqrt{\frac{1}{n}\sum_{i=1}^{n}(LST_i - T_{air,i})2}$$

where LST_i is the Landsat-derived land surface temperature and $T_{air,i}$ is the corresponding DHM air-temperature value. The results were interpreted as thermal-consistency indicators rather than direct LST retrieval errors.

2.8 CA–Markov modelling and 2030 scenario

The CA–Markov model was used to project a possible land use/land cover scenario for 2030. This approach combines the temporal transition capability of the Markov chain with the spatial allocation capability of Cellular Automata. The Markov component estimates the probability of conversion from

one land-cover class to another based on historical LULC changes, while the Cellular Automata component allocates these transitions spatially using neighbourhood relationships [17,18].

Before generating the 2030 scenario, the model was evaluated through a historical simulation. The classified LULC maps of 2014 and 2019 were used to simulate the 2024 LULC condition. The predicted 2024 map was then compared with the independently classified 2024 LULC map. Overall Accuracy and Kappa-based statistics were used to assess how well the model reproduced the observed 2024 land-cover pattern.

After validation, the calibrated CA–Markov model was used to generate the projected LULC scenario for 2030. Since land-cover change is one of the major drivers of surface thermal variation, the projected 2030 LULC map was further used to assess likely implications for LST and UHI intensity. The future thermal outputs were interpreted as scenario-based estimates rather than exact forecasts because future LST and UHI conditions may also be influenced by rainfall, humidity, wind, building materials, urban morphology, land-use policy, vegetation management, and broader climate variability.

2.9 Statistical and Spatial Analysis

Spatial and statistical analyses were carried out to compare LULC, NDVI, EVI, LST, and standardized UHI patterns for 2014, 2019, and 2024. Area statistics were calculated for each LULC class to quantify land-cover change over time. Minimum, maximum, and mean LST values were calculated for each study year to assess temporal variation in surface temperature.

Zonal statistics were applied using the annual LULC rasters as zone data and the corresponding LST rasters as value data. This allowed the mean LST of settlement, cultivation, forest, water bodies, and barren land to be calculated separately for each study year. The class-wise LST values were then used to examine the thermal behaviour of different land-cover types.

Correlation analysis was used to examine the relationships among NDVI, EVI, LST, and standardized UHI intensity. The relationship between LST and UHI was interpreted carefully because standardized UHI was mathematically derived from LST. Therefore, the LST–UHI relationship was considered a methodological relationship rather than an independent environmental finding.

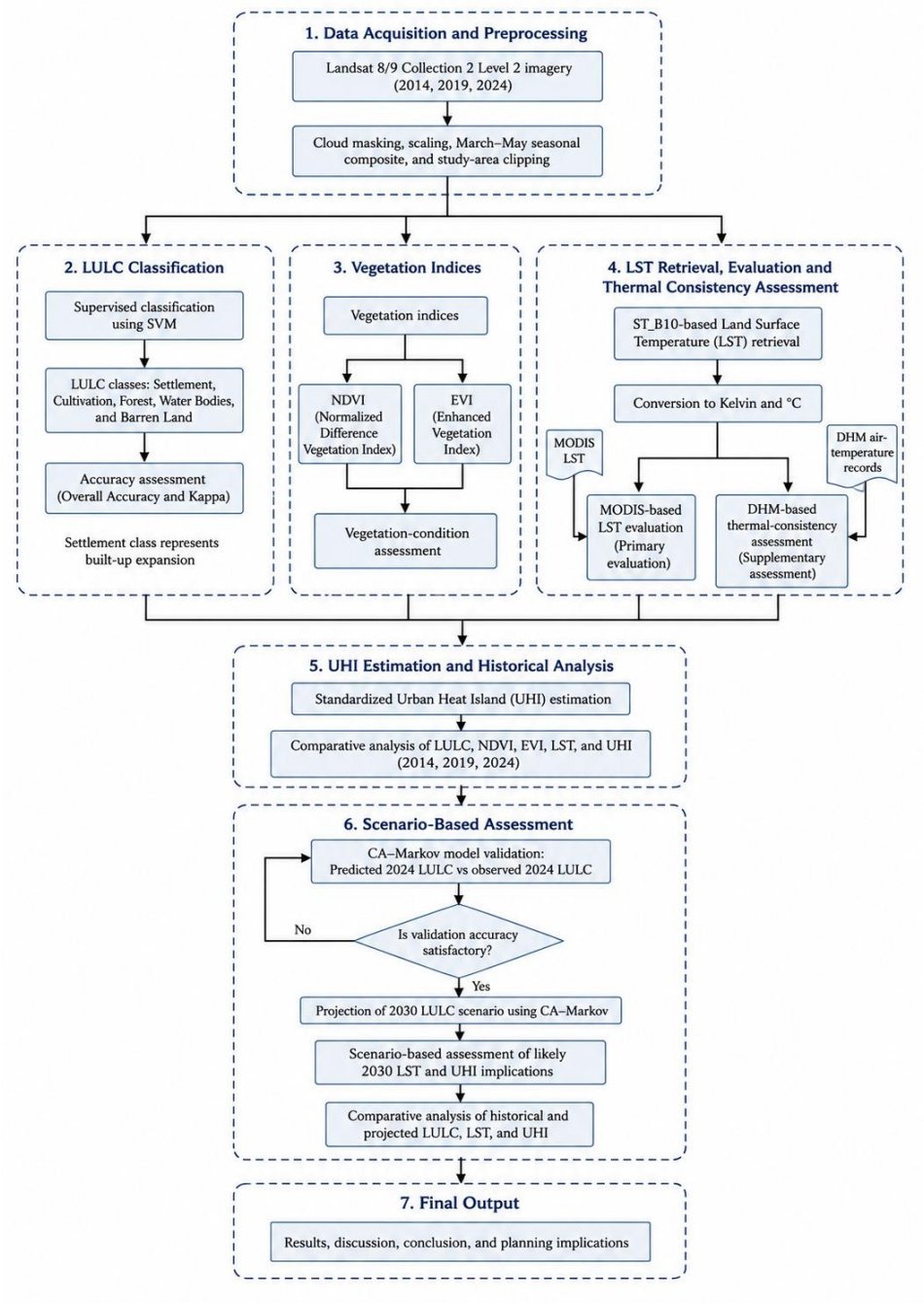


Fig. 2 Methodological workflow

3. Results

3.1 Land use and land cover change

The LULC classification results show a clear transformation of the selected core urban area of Pokhara between 2014 and 2024. In 2014, the study area was largely dominated by cultivation, which occupied 78.04% of the total area. Settlement covered 20.01%, while forest, water bodies, and barren land together occupied only a small proportion of the landscape.

By 2019, settlement increased to 29.57%, while cultivation declined to 63.95%. Barren land also increased from 0.37% in 2014 to 4.37% in 2019, indicating the expansion of exposed surfaces, construction areas, and transitional land. In 2024, settlement further increased to 37.45%, while cultivation declined to 55.53%. These results indicate that settlement expansion and cultivation loss were the dominant land-cover changes in the study area.

Between 2014 and 2024, settlement increased by 17.44 percentage points, representing an approximate relative increase of 87.16% compared with its 2014 coverage. Cultivation decreased by 22.51 percentage points during the same period. The LULC results therefore show a transition from a cultivation-dominated urban core toward a more built-up and impervious land-cover structure.

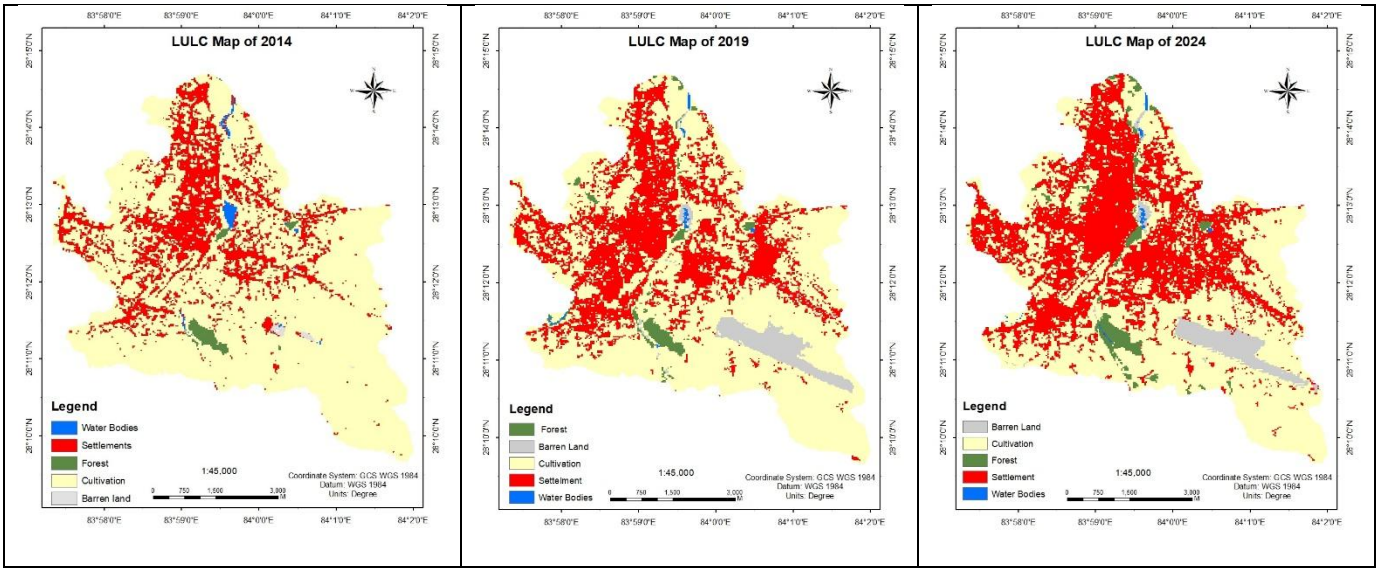


Table 2 Land use and land cover change from 2014 to 2024

LULC Class	2014		2019		2024	
	Area (sq. km)	Cover (%)	Area (sq. km)	Cover (%)	Area (sq. km)	Cover (%)
Cultivation	29.20	78.04	23.93	63.95	20.78	55.53
Settlement	7.49	20.01	11.07	29.57	14.01	37.45
Barren Land	0.14	0.37	1.64	4.37	1.54	4.11
Forest	0.38	1.03	0.68	1.83	0.99	2.64
Water Bodies	0.21	0.55	0.10	0.27	0.10	0.27
Total	37.42	100.00	37.42	100.00	37.42	100.00

The LULC classification accuracy was satisfactory for all three years. Overall Accuracy was 87.84% in 2014, 87.01% in 2019, and 85.29% in 2024. The Kappa coefficients were 0.8217, 0.8144, and 0.7888, respectively, indicating substantial to strong agreement between the classified maps and reference information.

3.2 Vegetation condition based on NDVI and EVI

The NDVI and EVI results show a gradual reduction in the spatial continuity of vegetation between 2014 and 2024. In 2014, higher vegetation-index values were more widely distributed across cultivated land, forest patches, and less-developed areas. By 2019, these higher-value areas became more

fragmented, while low vegetation-index values expanded around settlement, road corridors, airport-related surfaces, barren land, and exposed areas.

By 2024, high NDVI and EVI values were mainly limited to remaining cultivated land, forest patches, and localized vegetation areas. Low-index areas became more dominant across settlement and transitional surfaces. This indicates that urban expansion was accompanied not only by a reduction in cultivated land but also by increasing fragmentation of vegetation within the urban core.

The spatial pattern of NDVI and EVI was consistent with the LULC results. Areas with stronger vegetation signals generally corresponded with cultivation and forest classes, whereas settlement, barren land, airport-related surfaces, and exposed areas showed lower vegetation-index values.

3.3 Land surface temperature change

The LST results show a consistent increase in surface temperature between 2014 and 2024. In 2014, LST ranged from 23.54°C to 36.19°C, with a mean value of 29.87°C. In 2019, LST increased substantially, ranging from 26.64°C to 42.28°C, with a mean value of 34.46°C. By 2024, the LST range further increased from 30.34°C to 44.58°C, with a mean value of 37.46°C.

Between 2014 and 2024, minimum LST increased by 6.80°C, maximum LST increased by 8.39°C, and mean LST increased by 7.59°C. The warming pattern was spatially associated with settlement expansion, airport-related surfaces, barren land, construction areas, road corridors, and other exposed or sparsely vegetated surfaces. Relatively lower temperatures were mainly observed around forest patches, cultivated areas, and water-influenced locations.

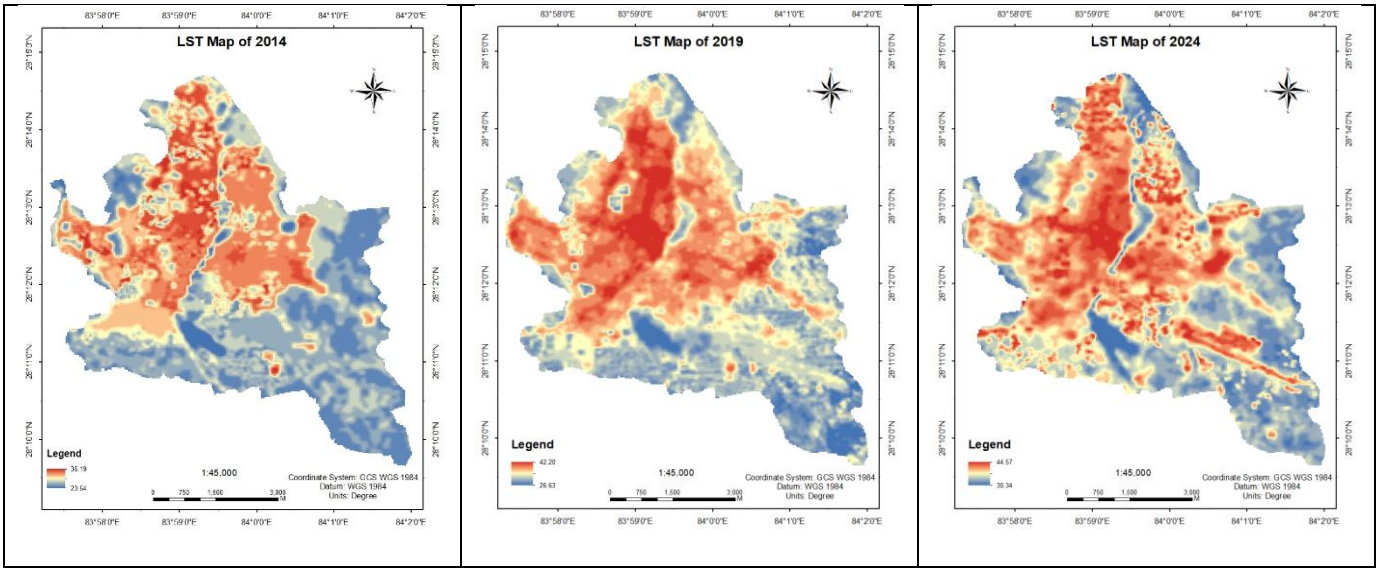


Fig. 4 LST maps of the selected core urban area of Pokhara for 2014, 2019, and 2024

Table 3 Land surface temperature statistics from 2014 to 2024

SN	Year	Minimum LST (°C)	Maximum LST (°C)	Mean LST (°C)
1	2014	23.54	36.19	29.87
2	2019	26.64	42.28	34.46
3	2024	30.34	44.58	37.46

3.4 Mean LST by land-cover class

Mean LST varied among the major LULC classes. In 2014, barren land recorded the highest mean LST of 34.51°C, followed by settlement at 33.37°C. Forest recorded the lowest mean LST at 29.08°C. In 2019 and 2024, settlement recorded the highest mean LST, increasing from 36.51°C in 2019 to 38.26°C in 2024. Forest maintained the lowest mean LST in all study years.

The class-wise results show that high surface temperature was not limited to settlement areas. Barren land and exposed surfaces also showed high thermal values because such surfaces generally contain

limited moisture and vegetation. Settlement and barren land were therefore the major contributors to high surface heating, while forest and other vegetated surfaces played a cooling role.

Table 4 Mean LST by land use and land cover class

Land Use/Land Cover Class	2014 Mean LST (°C)	2019 Mean LST (°C)	2024 Mean LST (°C)
Settlement	33.37	36.51	38.26
Cultivation	32.50	33.59	35.78
Forest	29.08	30.61	33.64
Water Bodies	32.42	31.92	33.95
Barren Land	34.51	33.47	37.29

3.5 Evaluation of Landsat-derived LST

Landsat-derived LST was evaluated using MODIS LST. The comparison showed a Pearson correlation coefficient of 0.736, indicating a moderately strong positive relationship between Landsat and MODIS LST. The RMSE was 2.79°C, showing reasonable cross-sensor agreement. The remaining differences may be related to differences in spatial resolution, sensor characteristics, acquisition time, mixed-pixel composition, and processing conditions.

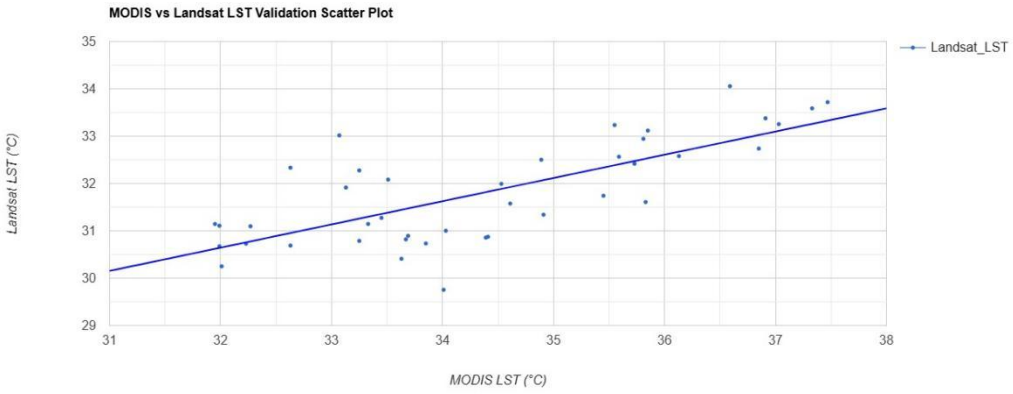


Fig. 5 Scatter plot showing the relationship between Landsat-derived LST and MODIS LST

A supplementary station-based thermal-consistency assessment was carried out using air-temperature records from Pokhara Airport Station. Landsat-derived LST at the station location increased from 30.452°C in 2014 to 34.119°C in 2019 and 36.228°C in 2024. Complete March–May DHM air-temperature values were available for 2019 and 2024. During this period, mean maximum air temperature increased from 28.704°C to 29.649°C, while mean air temperature increased from 22.412°C to 23.525°C.

The RMSE between Landsat LST and DHM maximum air temperature was 6.025°C, while the RMSE between Landsat LST and DHM mean air temperature was 12.215°C. These values were interpreted as numerical differences between land surface temperature and air temperature rather than direct LST retrieval errors, because LST and air temperature represent different physical measurements [16].

Table 5 Summary of LST evaluation and model-validation results

Evaluation component	**Metric**	**Value**	**Interpretation**
Landsat LST vs MODIS LST	Pearson correlation coefficient	0.736	Moderately strong positive relationship
Landsat LST vs MODIS LST	RMSE	2.79°C	Reasonable cross-sensor agreement
Landsat LST vs DHM Tmax	RMSE	6.025°C	LST higher than maximum air temperature
Landsat LST vs DHM mean air temperature	RMSE	12.215°C	Larger difference because mean air temperature includes cooler periods
CA–Markov LULC validation	Overall Accuracy	76.63%	Acceptable scenario-model performance
Predicted vs observed 2024 LST	RMSE	0.7906°C	Good agreement
Predicted vs observed 2024 UHI class	Overall Accuracy	72.68%	Good categorical agreement
Predicted vs observed 2024 UHI class	Kappa coefficient	0.725	Substantial agreement

3.6 Standardized UHI intensity

The standardized UHI maps show a progressive expansion of high-intensity thermal zones between 2014 and 2024. In 2014, High and Extremely High UHI zones were relatively localized and mainly associated

with settlement, airport-related surfaces, barren land, and exposed surfaces. By 2019, these zones expanded into newly developed and transitional areas. In 2024, High and Extremely High UHI zones became more widespread and spatially connected.

Low and Extremely Low UHI zones were mainly associated with forest patches, cultivated land, and water-influenced surfaces. The expansion of high UHI intensity corresponded with settlement growth, increasing impervious surfaces, exposed land, and fragmentation of vegetation. Since standardized UHI was calculated directly from each annual LST raster, the values represent relative thermal intensity and not direct urban–rural temperature differences in degrees Celsius.

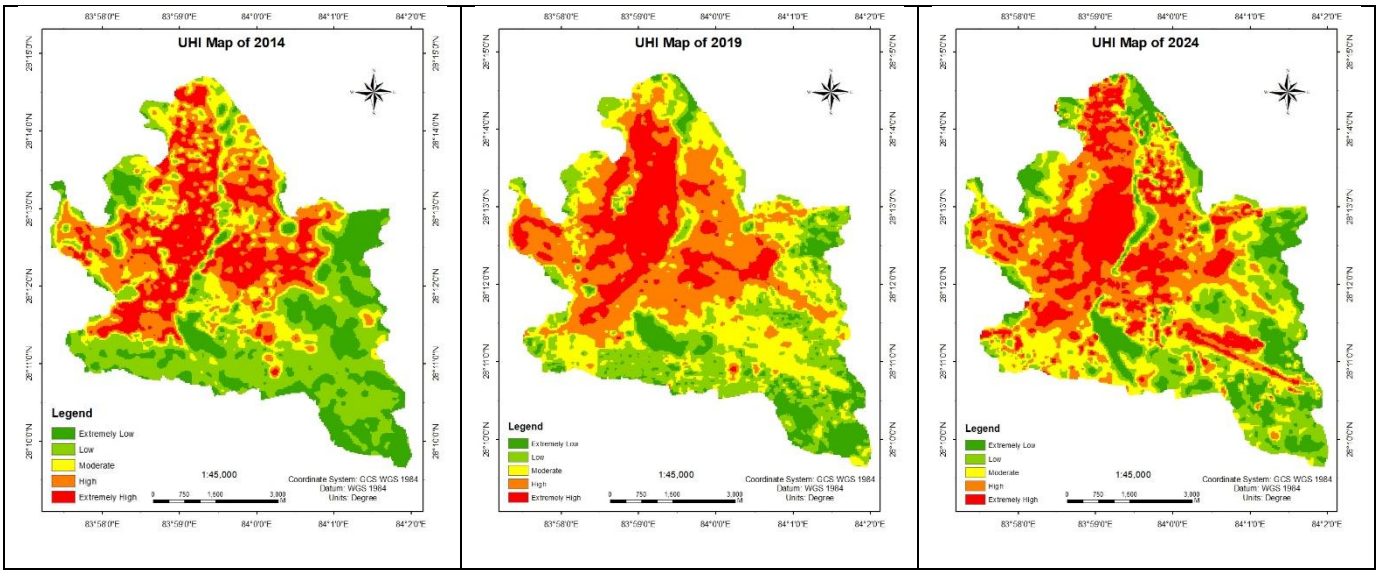


Fig. 6 Standardized UHI maps of the selected core urban area of Pokhara for 2014, 2019, and 2024

3.7 Relationship among vegetation, land cover, LST, and UHI

The combined analysis of NDVI, EVI, LULC, LST, and UHI shows that areas with stronger vegetation condition generally corresponded with lower LST and lower UHI intensity. Forest patches and cultivated land showed comparatively lower thermal values, while settlement, barren land, airport-related surfaces, construction areas, roads, and exposed dry land showed higher LST and higher standardized UHI values.

The relationship between vegetation indices and LST was negative, indicating that areas with higher vegetation greenness generally experienced lower surface heating. The relationship between LST and standardized UHI was strongly positive because UHI was mathematically derived from the LST raster. Therefore, the LST–UHI relationship was interpreted as a methodological relationship rather than an independent environmental relationship.

3.8 Model validation and 2030 scenario

Before generating the 2030 scenario, the CA–Markov model was evaluated by using the 2014 and 2019 LULC maps to simulate the 2024 LULC condition. The simulated 2024 map was compared with the independently classified 2024 map. The model achieved an Overall Accuracy of 76.63%, with Kno = 0.843, Klocation = 0.659, and Kstandard = 0.556. These results indicate acceptable agreement for scenario-based future projection.

The projected 2030 LULC scenario suggests that settlement and airport-related built-up surfaces may become the dominant land-cover category, occupying 50.43% of the study area. Cultivation is projected to decline to 45.99%, while forest may cover 3.01%, barren land 0.43%, and water bodies 0.13%. This indicates that future urban growth is likely to continue mainly through the conversion of cultivated and open surfaces into built-up and infrastructure-related land.

Table 6 Projected LULC distribution for 2030

LULC Class	Area (sq. km)	Percentage (%)
Settlement / Built-up including Airport	18.88	50.43
Cultivation	17.22	45.99
Forest	1.13	3.01
Barren Land	0.16	0.43
Water Bodies	0.05	0.13
Total	37.42	100.00

The projected standardized UHI scenario for 2030 indicates that High and Extremely High UHI classes may together occupy 50.63% of the selected core urban area. The High UHI class is projected to cover 26.78%, while the Extremely High UHI class may cover 23.85%. These zones are likely to be concentrated around dense settlement, airport-related built-up surfaces, transportation corridors, and exposed or impervious surfaces.

Table 7 Projected standardized UHI classification for 2030

UHI Class	Thermal intensity class	Area (km²)	Percentage (%)	Spatial Interpretation
1	Extremely Low	2.55	6.80	Water bodies / dense vegetation / cool zones
2	Low	6.53	17.46	Vegetated and low-density peripheral areas
3	Moderate	9.40	25.11	Suburban / transitional land-use zones
4	High	10.02	26.78	Dominant urban/built-up heat matrix
5	Extremely High	8.92	23.85	Urban core / strongest heat island hotspot

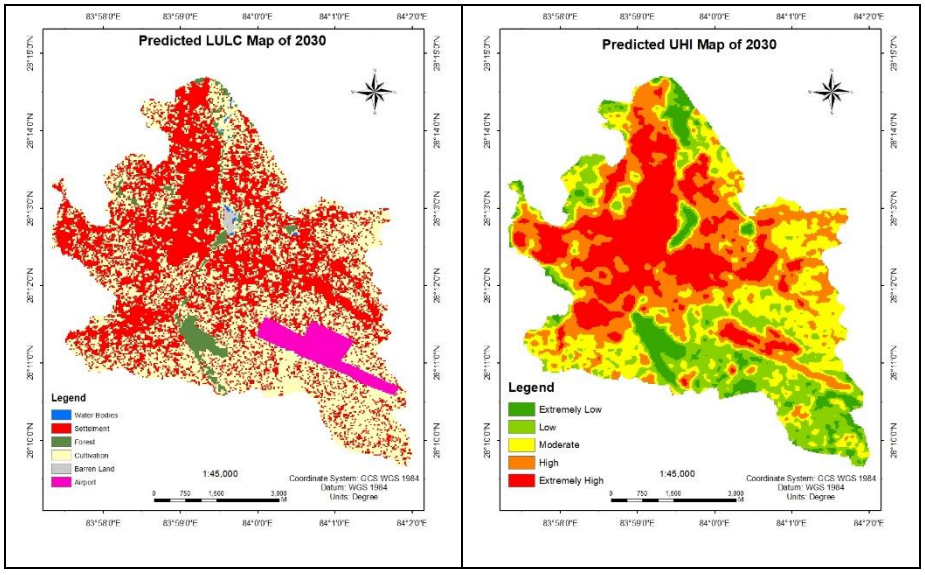


Fig. 7 Projected 2030 LULC and standardized UHI scenario for the selected core urban area of Pokhara

Overall, the 2030 scenario suggests that continued settlement expansion, cultivation decline, and growth of impervious and exposed surfaces may intensify the spatial extent of high UHI conditions in Pokhara's core urban area. However, the projected outputs should be interpreted as scenario-based estimates rather than exact forecasts, because future thermal conditions may also be influenced by climate variability, rainfall, humidity, wind, building materials, vegetation management, and planning decisions.

4. Discussion

The results show a clear transformation of Pokhara's core urban area from a cultivation-dominated landscape toward a more built-up and thermally intensified urban environment. Settlement increased from 20.01% in 2014 to 37.45% in 2024, while cultivation declined from 78.04% to 55.53%. This indicates that urban expansion in the selected core area has mainly occurred through the conversion of cultivated land and open surfaces into settlement, transport infrastructure, airport-related built-up areas, and other impervious or exposed surfaces. Such land-cover transformation is consistent with the general pattern of urban growth observed in rapidly developing cities, where vegetation and agricultural land are gradually replaced by built-up surfaces that store more heat [1,2].

The vegetation-index results further support this interpretation. NDVI and EVI patterns indicate that vegetation became increasingly fragmented between 2014 and 2024. Higher vegetation-index values were more widely distributed in 2014 but became more restricted to remaining cultivated land, forest patches, and localized green areas by 2024. In contrast, low NDVI and EVI values expanded across settlement, barren land, road corridors, airport-related surfaces, and exposed areas. This pattern confirms that urban expansion was accompanied not only by cultivation loss but also by reduced spatial continuity of vegetation. Since vegetation moderates surface heating through shading, evapotranspiration, and moisture retention, its fragmentation contributes to the intensification of surface temperature [3–5].

The LST results show substantial surface warming during the study period. Mean LST increased from 29.87°C in 2014 to 37.46°C in 2024, while maximum LST increased from 36.19°C to 44.58°C. The class-wise LST analysis showed that settlement and barren land generally recorded higher mean LST, whereas forest maintained the lowest mean LST in all study years. This indicates that high surface temperature in Pokhara is not limited only to dense settlement areas; exposed soil, construction areas, barren land, road corridors, and airport-related surfaces also contribute strongly to surface heating. Similar findings have been reported in Kathmandu Valley, where impervious surfaces, barren land, open land, and airport-related areas showed higher LST, while vegetation and water-influenced surfaces showed comparatively lower temperature [6,7,26–28]. The findings are also consistent with previous UHI-related work in Pokhara, which reported warmer conditions in urban areas compared with less-developed and vegetation-dominated locations [8].

The standardized UHI maps indicate that High and Extremely High thermal-intensity zones became more widespread and spatially connected between 2014 and 2024. These zones were mainly associated with settlement expansion, airport-related built-up surfaces, barren land, construction areas, road corridors, and other exposed or sparsely vegetated surfaces. Low and Extremely Low UHI zones were mostly associated with forest patches, cultivated land, and water-influenced surfaces. Since standardized UHI was derived from annual LST values, it represents relative thermal intensity within the study area rather than direct urban–rural temperature differences in degrees Celsius. Nevertheless, the expansion of high UHI classes clearly indicates increasing spatial concentration of surface heat in Pokhara's urban core.

The evaluation of Landsat-derived LST using MODIS LST showed reasonable cross-sensor agreement, with a Pearson correlation coefficient of 0.736 and RMSE of 2.79°C. This suggests that Landsat-derived LST captured the general spatial thermal pattern of the study area. Differences between Landsat and MODIS are expected because the two products differ in spatial resolution, acquisition characteristics,

sensor properties, and mixed-pixel composition [14,15]. The comparison with DHM air-temperature records was treated only as supplementary thermal-consistency evidence. The relatively higher RMSE values between Landsat LST and DHM air temperature should not be interpreted as direct LST retrieval errors because LST represents radiometric surface temperature, whereas air temperature represents near-surface atmospheric temperature measured at a station [16].

The CA–Markov-based 2030 scenario suggests that settlement and airport-related built-up surfaces may occupy 50.43% of the study area, while cultivation may decline to 45.99%. The projected standardized UHI result further indicates that High and Extremely High UHI classes may together cover 50.63% of the selected core urban area by 2030. These findings suggest that future urban heat may intensify if settlement expansion, cultivation loss, and exposed-surface growth continue without effective planning intervention. However, these outputs should be interpreted as scenario-based estimates rather than exact forecasts because future LST and UHI conditions may also be influenced by rainfall, humidity, wind, building materials, urban morphology, vegetation management, policy decisions, and broader climate variability [17,18].

Overall, the study highlights the need to integrate urban heat considerations into land-use planning in Pokhara. Protection of remaining cultivated land, forest patches, riparian areas, and open spaces is important for maintaining surface cooling. Urban greening should be combined with exposed-surface management, shaded corridors, cool paving materials, reflective roofing, and heat-sensitive infrastructure design. Areas projected to experience High and Extremely High UHI conditions should be prioritized for greening, surface-material improvement, and heat-risk monitoring. The results demonstrate that remote sensing, GIS, and scenario-based modelling can provide useful spatial evidence for climate-sensitive urban planning in rapidly developing mountain-valley cities.

5. Conclusion

This study assessed land use/land cover change, vegetation condition, land surface temperature, and standardized urban heat island intensity in the selected 37.42 km² core urban area of Pokhara Metropolitan City using Landsat imagery from 2014, 2019, and 2024. The results show a clear transformation from a cultivation-dominated landscape toward a more built-up and thermally intensified urban core.

Settlement increased from 20.01% in 2014 to 37.45% in 2024, while cultivation declined from 78.04% to 55.53%. This land-cover transformation was accompanied by vegetation fragmentation and expansion of impervious and exposed surfaces. During the same period, mean LST increased from 29.87°C to 37.46°C, while maximum LST increased from 36.19°C to 44.58°C. Class-wise analysis showed that settlement and barren land generally recorded higher mean LST, whereas forest consistently maintained the lowest mean LST, confirming the cooling role of vegetated surfaces.

The standardized UHI results indicate that High and Extremely High thermal-intensity zones became more extensive and spatially connected over time. These zones were mainly associated with settlement, airport-related built-up surfaces, barren land, road corridors, construction areas, and exposed dry surfaces. In contrast, lower UHI intensity was mainly linked with forest patches, cultivated land, and water-influenced areas. Since the UHI values were derived from standardized LST, they represent relative thermal intensity within the study area rather than direct urban–rural temperature differences.

The evaluation of Landsat-derived LST using MODIS LST showed reasonable cross-sensor agreement, with a Pearson correlation coefficient of 0.736 and RMSE of 2.79°C. DHM air-temperature records provided supplementary thermal-consistency evidence but were not treated as direct validation because land surface temperature and air temperature represent different physical measurements.

The CA–Markov-based 2030 scenario suggests that settlement and airport-related built-up surfaces may occupy 50.43% of the study area, while High and Extremely High UHI classes may together cover 50.63%. These findings indicate that continued settlement expansion, cultivation loss, and exposed-surface growth may further intensify urban heat conditions in Pokhara if appropriate planning measures are not implemented. Therefore, protection of remaining vegetation and cultivated land, development of connected green infrastructure, management of exposed surfaces, use of heat-sensitive materials, and regular remote-sensing-based thermal monitoring are important for reducing future UHI intensification in Pokhara's urban core.

Declarations

Funding

This research received no specific grant from any funding agency in the public, commercial, or not-for-profit sectors.

Ethics approval and consent to participate

Not applicable. This study did not involve human participants, animal subjects, clinical data, interviews, household surveys, or personally identifiable information.

Consent for publication

Not applicable.

Competing interests

The author declares that there are no competing financial or non-financial interests related to this work.

Author contributions

Bhuwan Singh Bisht conceptualized the study, designed the methodology, collected and processed the satellite and ancillary datasets, performed the remote sensing and GIS analyses, interpreted the results, prepared the figures and tables, and wrote the original manuscript. Dr. Hemu Kafle supervised the research, contributed to the study design, provided scientific guidance, reviewed and edited the manuscript, and validated the findings. Amit Yadav assisted with data interpretation, reviewed the methodology, and contributed to manuscript editing. Sushil Subedi contributed to data checking, result verification, manuscript review, and editing. Gaurav Bisht contributed to data validation, visualization, manuscript review, and editing.

Third-party material

The manuscript does not contain any copyrighted third-party figures, images, maps, or supplementary materials. All figures, maps, tables, and analysis outputs were prepared by the author using publicly available datasets and the author's own analysis.

Data availability

The satellite datasets used in this study are publicly available through Google Earth Engine, including Landsat Collection 2 Level 2 imagery and MODIS LST products. Administrative boundary data were obtained from the National Geoportal of Nepal. Air-temperature records used for supplementary thermal-consistency assessment were obtained from the Department of Hydrology and Meteorology, Nepal. The processed datasets and analysis outputs generated during the study are available from the corresponding author upon reasonable request.

Acknowledgements

The author acknowledges the Department of Hydrology and Meteorology, Nepal, for providing air-temperature records used in this study. The author also acknowledges Google Earth Engine, Landsat, MODIS, and the National Geoportal of Nepal for providing access to satellite and spatial datasets. The author is grateful to Nepal Open University and the Department of Geoinformatics for academic support during the research.

References

[1] Arnfield AJ. Two decades of urban climate research: a review of turbulence, exchanges of energy and water, and the urban heat island. International Journal of Climatology. 2003;23(1):1–26. https://doi.org/10.1002/joc.859

[2] Voogt JA, Oke TR. Thermal remote sensing of urban climates. Remote Sensing of Environment. 2003;86(3):370–384. https://doi.org/10.1016/S0034-4257(03)00079-8

[3] Weng Q, Lu D, Schubring J. Estimation of land surface temperature–vegetation abundance relationship for urban heat island studies. Remote Sensing of Environment. 2004;89(4):467–483. https://doi.org/10.1016/j.rse.2003.11.005

[4] Huete A, Didan K, Miura T, Rodriguez EP, Gao X, Ferreira LG. Overview of the radiometric and biophysical performance of the MODIS vegetation indices. Remote Sensing of Environment. 2002;83(1–2):195–213. https://doi.org/10.1016/S0034-4257(02)00096-2

[5] Tucker CJ. Red and photographic infrared linear combinations for monitoring vegetation. Remote Sensing of Environment. 1979;8(2):127–150. https://doi.org/10.1016/0034-4257(79)90013-0

[6] Sarif MO, Rimal B, Stork NE. Assessment of changes in land use/land cover and land surface temperatures and their impact on surface urban heat island phenomena in Kathmandu

Valley, 1988–2018. ISPRS International Journal of Geo-Information. 2020;9(12):726. https://doi.org/10.3390/ijgi9120726

[7] Karunaratne S, Athukorala D, Murayama Y, Morimoto T. Assessing surface urban heat island related to land use/land cover composition and pattern in the temperate mountain valley city of Kathmandu, Nepal. Remote Sensing. 2022;14(16):4047. https://doi.org/10.3390/rs14164047

[8] Jamarkattel U, Lamichhane BR, Gautam S, Horanont T. Analyzing urban heat islands in Pokhara Metropolitan City–Nepal through remote sensing techniques. SSRN Preprint. 2024. https://doi.org/10.2139/ssrn.4980837

[9] Gorelick N, Hancher M, Dixon M, Ilyushchenko S, Thau D, Moore R. Google Earth Engine: planetary-scale geospatial analysis for everyone. Remote Sensing of Environment. 2017;202:18–27. https://doi.org/10.1016/j.rse.2017.06.031

[10] Cortes C, Vapnik V. Support-vector networks. Machine Learning. 1995;20:273–297. https://doi.org/10.1007/BF00994018

[11] United States Geological Survey. How do I use a scale factor with Landsat Level-2 science products? U.S. Geological Survey. Available from: https://www.usgs.gov/faqs/how-do-i-use-a-scale-factor-landsat-level-2-science-products

[12] Abutaleb K, Ngie A, Darwish A, Ahmed M, Arafat S, Ahmed F. Assessment of urban heat island using remotely sensed imagery over Greater Cairo, Egypt. Advances in Remote Sensing. 2015;4(1):35–47. https://doi.org/10.4236/ars.2015.41004

[13] Malakar NK, Hulley GC, Hook SJ, Laraby K, Cook M, Schott JR. An operational land surface temperature product for Landsat thermal data: methodology and validation. IEEE

Transactions on Geoscience and Remote Sensing. 2018;56(10):5717–5735. https://doi.org/10.1109/TGRS.2018.2824828

[14] Wan Z, Hook S, Hulley G. MODIS/Terra land surface temperature/emissivity daily L3 global 1 km SIN grid V061 [Data set]. NASA EOSDIS Land Processes Distributed Active Archive Center. 2021. https://doi.org/10.5067/MODIS/MOD11A1.061

[15] Phan TN, Kappas M. Application of MODIS land surface temperature data: a systematic literature review and analysis. Journal of Applied Remote Sensing. 2018;12(4):041501. https://doi.org/10.1117/1.JRS.12.041501

[16] Mildrexler DJ, Zhao M, Running SW. A global comparison between station air temperatures and MODIS land surface temperatures reveals the cooling role of forests. Journal of Geophysical Research: Biogeosciences. 2011;116(G3):G03025. https://doi.org/10.1029/2010JG001486

[17] Pontius RG Jr, Malanson J. Comparison of the structure and accuracy of two land change models. International Journal of Geographical Information Science. 2005;19(2):243–265. https://doi.org/10.1080/13658810410001713434

[18] Hamad R, Balzter H, Kolo K. Predicting land use/land cover changes using a CA–Markov model under two different scenarios. Sustainability. 2018;10(10):3421. https://doi.org/10.3390/su10103421

[19] Rajkarnikar A, Salike I. Urban heat island in Kathmandu Valley: a case of Patan. Proceedings of IOE Graduate Conference. 2020;8:394–400.

[20] Thapa RB. A study of urban heat island relating local climate zones using Landsat images: the case of Kathmandu Valley. Himalayan Journal of Applied Science and Engineering. 2021;2(1):59–69.

[21] Khatri B, Kharel B, Dhakal P, Acharya S, Thapa U. Spatio-temporal dynamics of urban heat island using Google Earth Engine: assessment and prediction—A case study of Kathmandu Valley, Nepal. Climate Services. 2025;38:100560. https://doi.org/10.1016/j.cliser.2025.100560